

High Performance, Flexible, and Thermally Stable All-Solid-State Organic Electrochemical Transistor Based on Thermoplastic Polyurethane Ion Gel

Kunqi Hou, Shuai Chen, Akshay Moudgil, Xihu Wu, Teck Lip Dexter Tam, Wen Siang Lew,* and Wei Lin Leong*

Cite This: *ACS Appl. Electron. Mater.* 2023, 5, 2215–2226

Read Online

ACCESS |

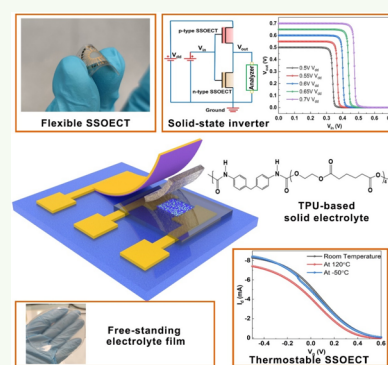
Metrics & More

Article Recommendations

Supporting Information

ABSTRACT: Organic electrochemical transistors (OECTs) are a generation of transistors with high transconductance, where the whole volume of the semiconducting channel is involved in the electrochemical doping process. However, the use of liquid electrolytes limits the application of OECTs, and the doping process is also complicated due to the presence of water in the electrolyte. In this study, thermoplastic polyurethane (TPU)-based solid electrolyte was used in OECTs for the first time. Three types of ionic liquids were blended with a TPU polymer matrix as a solid electrolyte and investigated on the OECTs based on three kinds of p-type conjugated semiconductors. An in situ spectrochemistry study was further carried out to confirm the doping/dedoping process of these conjugated semiconductors by the TPU-based solid electrolyte. The robustness and high stability of the fabricated solid-state OECTs (SSOECTs) were demonstrated through continuously applied bias, long time operation under ambient conditions, and varying temperatures (−50 to 120 °C). Highly flexible SSOECTs were also obtained on a polyethylene terephthalate (PET) substrate, which showed negligible fluctuation in on/off-current ($I_{\text{on}}/I_{\text{off}}$) after 1000 cycles of bending. Based on these high-performing SSOECTs, inverter circuits were fabricated in both unipolar and complementary configurations, where n-type and p-type OECT-based complementary inverters showed a higher gain (46) compared with that of the unipolar design.

KEYWORDS: organic electrochemical transistor, solid electrolyte, ionic liquid, complementary inverter, flexible electronics



1. INTRODUCTION

The organic electrochemical transistor (OECT) is of great interest due to its high transconductance and low driving voltage (<1 V), which enable its application in bioelectronics, logic circuit elements, and neuromorphic computing.^{1–6} It consists of a conjugated semiconductor directly in contact with an electrolyte. OECTs rely on the electrochemical doping effect, where the ions are injected from the electrolyte into the conjugated semiconductor film, therefore changing its doping state and alternating the conductivity of the channel.⁷ The carrier density in the channel is modulated by an applied gate bias (V_g), and the doping state of the semiconductor can be observed by the change in drain current (I_d) under an applied drain voltage (V_d).⁸ The gradient of the change of I_d versus V_g is defined as transconductance (g_m). Since the whole volume of the channel was induced in the ionic doping process, a significant modulation in drain current can be achieved under a low applied gate bias.⁹ OECTs are known as efficient switches and powerful amplifiers because ionic doping occurs over the entire volume of the channel layer, and significant modulations in the source-drain current can be achieved under low-gate voltages, as opposed to a thin interfacial region in field-effect transistors.

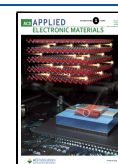
However, the device structure, especially the use of liquid or aqueous electrolyte, limits further application in wearable devices and electronic skins (E-skins). Although liquid electrolytes can allow high operational stability in some studies, the long-term device performance can change over time due to liquid evaporation. On the other hand, possible leakage of the electrolytes is an issue, and a high cost in device encapsulation is inevitable. Moreover, it is difficult to fabricate high-density and flexible OECT devices due to the liquid electrolytes and packaging issues.^{10–13} Therefore, the development of a solid-state electrolyte is necessary and enables long-term performance stability, which can further extend the applications in wearable sensor devices and E-skins.^{14,15}

There are several studies on the utilization of solid polyelectrolyte as the ion reservoir for OECTs. For instance, poly(sodium 4-styrenesulfonate) (PSS:Na) has been shown to

Received: January 20, 2023

Accepted: March 26, 2023

Published: April 7, 2023



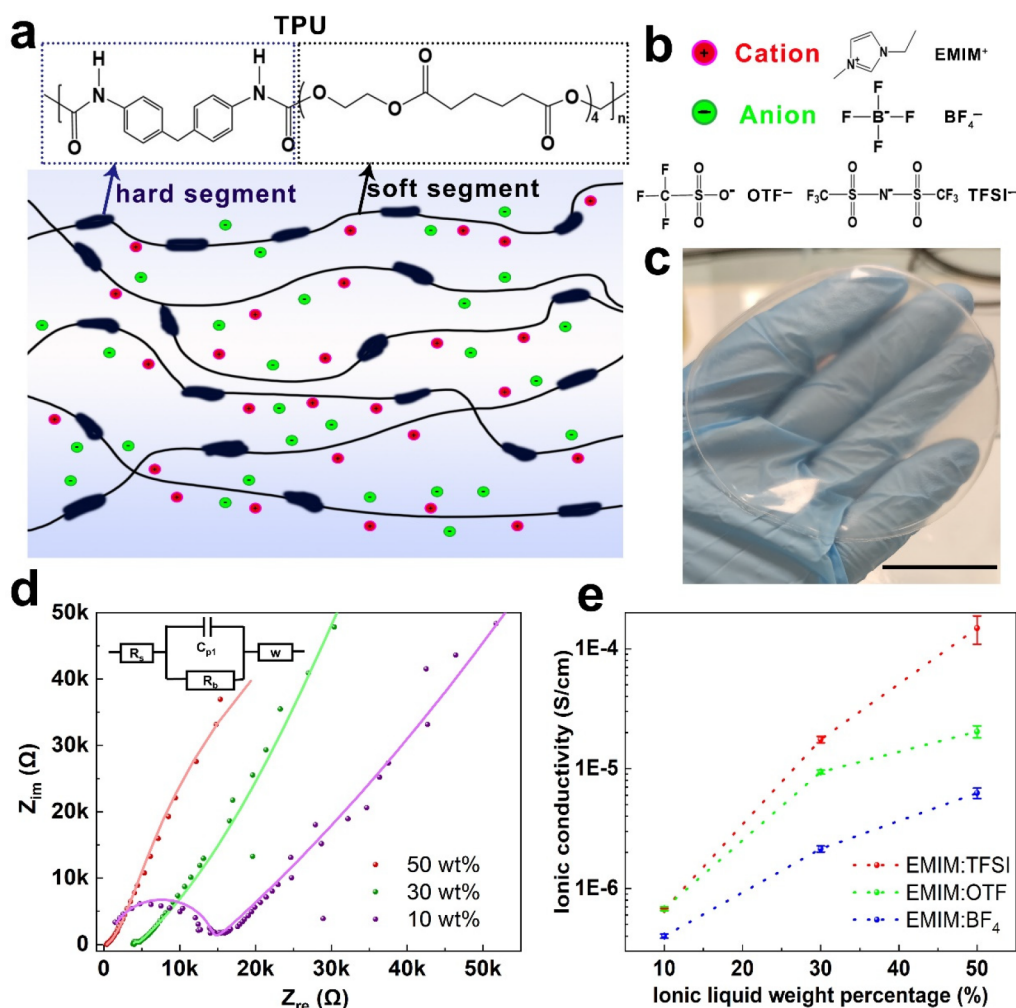


Figure 1. Introduction and characterization of TPU ionic gel. (a) Molecular structure and schematic illustration on TPU. (b) Molecular structures of cations and anions used in this study. (c) Fabricated free-standing SPE film with 30 wt % EMIM:TFSI (scale bar: 5 cm). (d) Nyquist plots of SPE containing EMIM:TFSI and an equivalent circuit used for fitting in ionic conductivity measurement. Solid lines are the fitting curves using an equivalent circuit. (e) Comparison of the ionic conductivities by using three types of anions in concentrations of 10, 30, and 50 wt %.

be a solid electrolyte for both n-type and p-type semiconductors.^{16,17} However, the PSS⁻ backbone has a strong electrostatic force on sodium cations, which induces higher activation energy and therefore resulted in higher threshold voltage (V_{th}) in OECT operation.¹⁸ Another type of solid-state electrolyte is generated by mixing the ionic source into a polymer matrix. Poly(vinylidene fluoride)-*co*-hexafluoropropylene (PVDF-HFP) has been widely used to be the polymer backbone of solid electrolytes of OECTs in many studies due to its high ionic conductivity.^{18,19} Melianas et al. reported an OECT-based synaptic device using this electrolyte, which can be operated stably from 30 to 90 °C.²⁰ But at a high concentration of ionic liquid, the PVDF-HFP ionic gel starts to melt above 100 °C, which limits the scope of applications of SSOECTs.²¹ The devices need to be robust under various temperature environments in practical applications. There are not many reports on the temperature robustness in OECTs. Han et al. reported a dual-network electrolyte based on cross-linked polyacrylamide and carrageenan for OECTs, which showed a stable switching down to -30 °C.²² However, there is a shift in threshold voltage at low temperatures and incomplete data under high-temperature conditions. Recently, thermoplastic polyurethane (TPU) has been investigated as a

promising polymer electrolyte for lithium batteries and free-standing transistors due to its high melting point (146 °C), ionic conductivity, and elasticity.^{23–29} However, such a host polymer has not been explored as an electrolyte for OECT devices.

In this work, we demonstrate for the first time the use of TPU as a solid polymer electrolyte (SPE) for OECT devices. The effect of three types of ionic liquid-induced doping on the g_m , V_{th} , and response time of PEDOT:PSS-based solid-state OECT (SSOECT) was investigated. PEDOT:PSS-based OECTs have been demonstrated for printable electronics and bioelectronics,^{30,31} and the morphology of the PEDOT:PSS channel is critical for the performance of OECTs.^{32,33} Herein, we successfully improved the performance of PEDOT:PSS-based OECTs through electrolyte-composite engineering and morphology tuning via electrolyte solvent treatment. The resulting OECTs showed excellent electrical, long-term, and temperature stability. Highly flexible OECT was also achieved and could retain its current value even after bending down to a 10 mm radius of curvature (ROC), which showed potential applications of our devices for wearable electronics and bioelectronics.

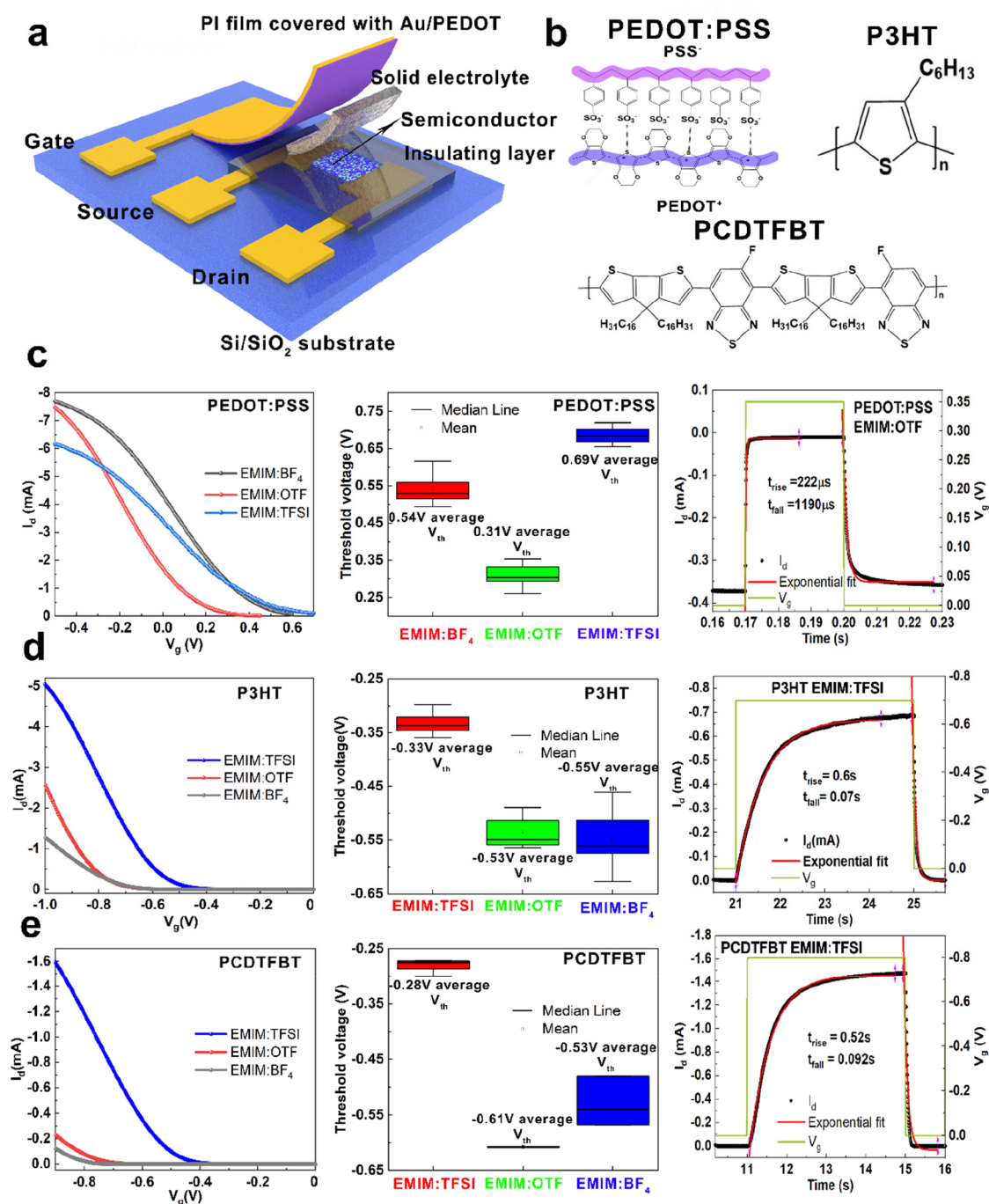


Figure 2. Characterization of SSOECTs utilizing TPU-based ionic gel as a solid electrolyte, where ionic concentration of the electrolyte was kept at 50 wt % for all SSOECTs. Thickness (d) of the semiconductors is 107, 109, and 81 nm for PEDOT:PSS, P3HT, and PCDTFBT, respectively. (a) Schematic diagram of fabricated SSOECT device. (b) Molecular structure of conjugated semiconductors (PEDOT:PSS, P3HT, PCDTFBT). (c–e) Forward-scan transfer curves, average threshold voltages, and transient response of PEDOT:PSS, P3HT, and PCDTFBT-based SSOECTs using BF₄⁻, OTF⁻, and TFSI⁻ as anions. A -0.5 V drain voltage was applied during the measurement, and a 0.5 V drain voltage was applied for all n-type OECTs. And the average V_{th} results were calculated among 10 devices.

Going beyond conventional PEDOT:PSS, we extend our studies to a representative variety of ion-permeable conjugated polymers, namely, poly(3-hexythiophene-2,5-diyl) (P3HT), poly[(5-fluoro-2,1,3-benzothiadiazole-4,7-diyl)(4,4-dihexadecyl-4H-cyclopenta[2,1-b:3,4-b']dithiophene-2,6-diyl)(6-fluoro-2,1,3-benzothiadiazole-4,7-diyl)(4,4-dihexadecyl-4H-cyclopenta[2,1-b:3,4-b']dithiophene-2,6-diyl)] (PCDTFBT), and poly(benzimidazobenzophenanthroline) (BBL). The generality of our approach allows the field of OECTs to grow rapidly

by harnessing the myriad of organic semiconductors developed for organic field-effect transistors (OFETs) but deemed unsuitable for OECT due to their aqueous instability. In situ electrochemical spectroscopy studies were also carried out to demonstrate and prove the electrochemical doping process in these conjugated polymers by TPU electrolyte. Finally, both n- and p-type SSOECTs are integrated for complementary inverter circuits, which achieved a gain factor of 46, significantly higher as compared with that for unipolar design.

2. RESULTS AND DISCUSSION

Figure 1a shows the molecular structure and schematic illustration of TPU. It consists of a two-phase microstructure, a soft (line chain) and hard (solid rings) segment, which makes it a favorable material for polymer electrolytes.^{34–36} The soft segment can reduce the combination force between cations and anions and give rise to good ionic transport,^{37,38} while the hard segment with high polarity can allow the electrolyte film to have good mechanical and physical properties such as high flexibility and thermal stability.^{39,40} We employ three different ionic sources in the TPU matrix, as shown in Figure 1b, namely, 1-ethyl-3-methylimidazolium tetrafluoroborate (EMIM:BF₄), 1-ethyl-3-methylimidazolium trifluoromethanesulfonate (EMIM:OTF), and 1-ethyl-3-methylimidazolium bis(trifluoromethyl sulfonyl) amide (EMIM:TFSI). The EMIM⁺ cation is widely used to dope or dedope the organic semiconductor.^{14,19,41} Both bis(trifluoromethanesulfonyl)-imide (TFSI⁻) and trifluoromethanesulfonate (OTF⁻) anions have a weak binding affinity with EMIM⁺ cations and a good plasticizing ability for the polymer backbone, while tetrafluoroborate (BF₄⁻) has a smaller size, which permits it to dope the organic semiconductor quickly and may have the potential to attain a lower threshold voltage and fast transient response. The miscibility of these ionic liquids with the TPU polymer is good, where free-standing electrolyte films with high transparency were obtained (see Figure 1c). The pure TPU film and after adding ionic liquid were characterized by field-emission scanning electron microscopy (FESEM), shown in Figure S1. Mixing the ionic liquid with the TPU polymer matrix significantly changed the surface topography, where a phase separation between soft and hard segments is more obvious than pure TPU film.

Electrochemical impedance spectroscopy (EIS) measurements were first carried out to study the ionic conductivity of these SPEs.^{42,43} SPE films with three types of ionic liquids in varying concentrations of 10, 30, and 50 wt % were measured, and the typical Nyquist plot using EMIM:TFSI is shown in Figure 1d (plots for other ionic liquids/TPU are shown in Figure S2). The semicircle in the plot is attributed to the ionic conduction of SPEs, where its diameter reflects the sum of the contact resistance (R_c) and the bulk resistance (R_b) of the device (Figure S3).⁴⁴ The ionic conductivities are summarized in Figure 1e. In general, the ionic conductivity of the electrolyte films is found to be proportional to the concentration of the ionic liquids. EMIM:TFSI is found to have the highest ionic conductivity (1.48×10^{-4} S cm⁻¹), while EMIM:BF₄ displayed the lowest ionic conductivity (6.26×10^{-6} S cm⁻¹) at 50 wt %. This correlates well with the weak binding affinity between TFSI⁻ and EMIM⁺ as compared to BF₄⁻ and EMIM⁺,⁴⁵ where the lower binding energy enables ions to move easier inside the polymer matrix.⁴⁶ The average ionic conductivities and their standard deviations are also presented in Table S1.

Figure 2a shows the schematic demonstration of the fabricated SSOECT on silicon oxide (SiO₂) substrate. Three types of conjugated semiconducting materials (PEDOT:PSS, P3HT, and PCDTFBT) were investigated in this study (Figure 2b), to demonstrate the generality of TPU-based ionic gel for OECTs. TPU-based solid electrolyte was directly spin-coated on top of these semiconductor channels, followed by placing a polyimide film coated with Au/PEDOT:PSS on top as the gate electrode. The optical image of the fabricated OECT channel

based on pristine PEDOT:PSS is shown in Figure S4. OECT with channel dimensions of $W/L = 100 \mu\text{m}/10 \mu\text{m}$ was chosen for the following experiments if there is no special mention.

PEDOT:PSS is a typical p-type semiconductor used as the active material for characteristics, and a comparison of the average V_{th} of PEDOT-based transistors using different anions is shown in Figure 2c and Figures S5–S7. The SSOECT performance was found to depend heavily on the type of anions in the solid electrolyte, where BF₄⁻ and OTF⁻ anions give larger I_{on} (~ 7.8 mA) than TFSI⁻ (6.2 mA) under negative gate bias. Moreover, the TFSI⁻ anion shows the highest average V_{th} (0.69 V), while the average V_{th} for BF₄⁻ and OTF⁻ were 0.54 and 0.31 V, respectively. The V_{th} shifting depends on the ionic hydrophilicity, where highly hydrophilic OTF⁻ anions contribute to easier ionic transport from the electrolyte to semiconductors.⁴⁷ Notably, the V_{th} of 0.31 V using TPU/EMIM:OTF as an electrolyte is lower than most of the reported PEDOT:PSS-based OECTs using a NaCl aqueous electrolyte,⁴⁸ which might be due to this anion having a weak binding affinity with EMIM⁺ cations and resulting in good ion transport between a solid electrolyte and channel. Therefore, the shortest rise time (defined as τ) of 222 μs was obtained using such anions as shown in Figure 2c. Pure TPU film (without ions) was also utilized in the device, but no gate-modulation effect in drain current was observed, which indicates that the transistor relied on electrochemical doping rather than field effect, and ionic liquids played the role in doping/dedoping processes (Figure S8).

Another interesting observation is that the measured PEDOT:PSS channel exhibits high conductivity, which resulted from the post-treatment during the spin-coating process of the solid electrolyte.⁴⁹ Since the electrolyte solution was directly spin-coated onto a PEDOT:PSS channel and the solvent used for the TPU electrolyte is dimethylformamide (DMF), the morphology of the PEDOT:PSS channel can be simultaneously tuned during the formation of SPE film.^{50–52} DMF solvent has been reported to enhance the conductivity of PEDOT:PSS by Dong and Portale, where high polarity solvent will decrease PSS–PSS interaction and transfer the molecular structure from a globular core–shell structure to an elongated fibrous network.⁵⁰ To confirm this hypothesis, we compared two OECT devices (gated by 0.1 M NaCl liquid electrolyte), where one of the PEDOT:PSS channels was treated by DMF solvent. The channel conductivity and g_m increased by 3 orders of magnitude for the PEDOT:PSS channel treated by DMF solvent (see Figure S9). The AFM phase images in Figure S10 presented a significant phase separation between PEDOT and PSS on solvent-treated film as compared with the pristine film. Therefore, for our PEDOT:PSS-based SSOECTs, the combination of TPU ionic gel with high ionic conductivity and post-treatment effect on the PEDOT:PSS morphology leads to a highly improved normalized transconductance (10.43 mS μm^{-1} for BF₄⁻ and 10.31 mS μm^{-1} for OTF⁻), which is much higher than most of the reported SSOECTs and even aqueous electrolyte-based OECTs (Table S2, Supporting Information).^{53,54}

To further explore the accessibility of TPU-based solid electrolytes, we extend our studies to P3HT and PCDTFBT, which are widely used as enhancement mode semiconductors for OECTs (Figures S11–S13). The injection of anions into these semiconductors induces more holes as charge carriers under a negative gate bias, thus improving their conductivity. The transfer characteristics and the comparison of average V_{th}

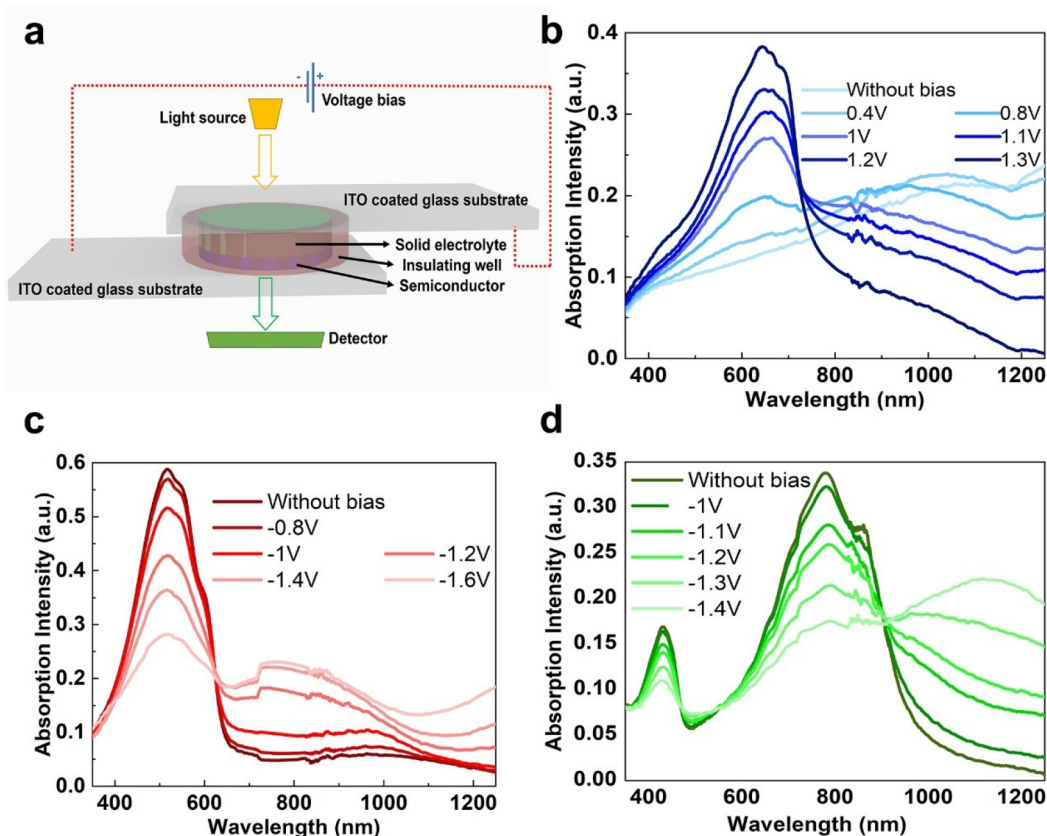


Figure 3. In situ UV–vis absorption spectra of PEDOT, P3HT, and PCDTFBT systems. (a) Schematic diagram of measurement setup, and structure of the fabricated sample. (b–d) Absorption spectra of PEDOT, P3HT, and PCDTFBT films under varying doping states. 50 wt % EMIM:OTF was blended with TPU polymer as a solid electrolyte for the PEDOT:PSS system, while 50 wt % EMIM:TFSI was blended with TPU polymer as a solid electrolyte for the P3HT and PCDTFBT systems due to a lower V_{th} , which more easily triggers doping at a lower voltage bias.

of P3HT and PCDTFBT-based transistors using three types of anions are shown in Figure 2d and e, respectively. In contrast to PEDOT:PSS-based OECTs, the TFSI[−] anion appears to be more effective in doping the channel where a lower V_{th} was obtained (−0.33 V for P3HT and −0.28 V for PCDTFBT), while both BF₄[−] and OTF[−] showed a much higher V_{th} of −0.55 V for both semiconductors. The differences in ionic doping capability are probably related to the hydrophilicity/hydrophobicity of these anions.⁵⁵ The hydrophobic anion (TFSI[−]) has a larger tendency to combine with hydrophobic channels (P3HT/PCDTFBT) as compared with hydrophilic anions (BF₄[−] and OTF[−]), which will induce higher hole mobility and lower V_{th} .⁵⁶ A statistical study on the g_m , τ , and μC^* (μ is charge-carrier mobility, C^* is volumetric capacitance) of these conjugated semiconductor-based SSOECTs (Figure S14) also corroborates this finding. The τ was obtained to be 0.52 s for P3HT and 0.6 s for PCDTFBT while using a TFSI-based SPE (Figure 2d and e). Surprisingly, P3HT-based SSOECTs using all kinds of ionic liquids showed >10⁶ on–off ratios, where the semilog transfer characteristics of these semiconductors are shown in Figure S15 to present the drain current on–off ratios. All of these devices showed a small degree of hysteresis in their transfer characteristics due to the delayed ionic–electronic interactions at the electrolyte–semiconductor interface (Figure S16).⁴¹ A thickness-dependent study of the channels was also conducted, which confirms the volumetric doping of these materials (Figure S17). Additionally, an n-type semiconductor, BBL, was utilized, where cations (EMIM⁺) will dope the redox-active sites of BBL

and generate electrons under the positive gate bias (Figure S18). These results further confirm the generality of our solid electrolyte for conjugated semiconductors.

In situ spectrochemical studies were further carried out to confirm the doping/dedoping process of conjugated semiconductors by a TPU-based solid electrolyte. An indium tin oxide (ITO)/SPE/conjugated semiconductor/ITO sandwich structure was built up, as shown in Figure 3a. For the PEDOT:PSS film, an absorption peak at a wavelength ranging from 600 to 700 nm appeared due to the π – π^* transition of neutral PEDOT after applying a positive gate bias, as shown in Figure 3b. As a result, the absorption in the infrared (IR) region dropped accordingly due to the reduced polaron transition.^{57,58} For P3HT and PCDTFBT, the initial absorption peaks were 500 and 450 nm/750 nm, respectively, which attributed to the π – π^* transition (Figure 3c and d). By applying negative bias beyond −1 V, anions were pushed into the semiconductor film, and subsequently, the doping state changed from neutral to an oxidized state. As a result, the absorption peaks shifted to the near-infrared region, and the films appeared more transparent.

Long-term operational stability for aqueous electrolyte-based OECTs still remains a challenge, as their solvent can evaporate over time. SSOECT with nonvolatile ion gel enables its reliability and long-term operation. Herein, characterizations of our PEDOT:PSS-based SSOECT in terms of electrical stability, long-term stability, and temperature resilience were carried out. First, five continuous DC cycles of double-sweep transfer curves were obtained, as shown in Figure 4a, where the

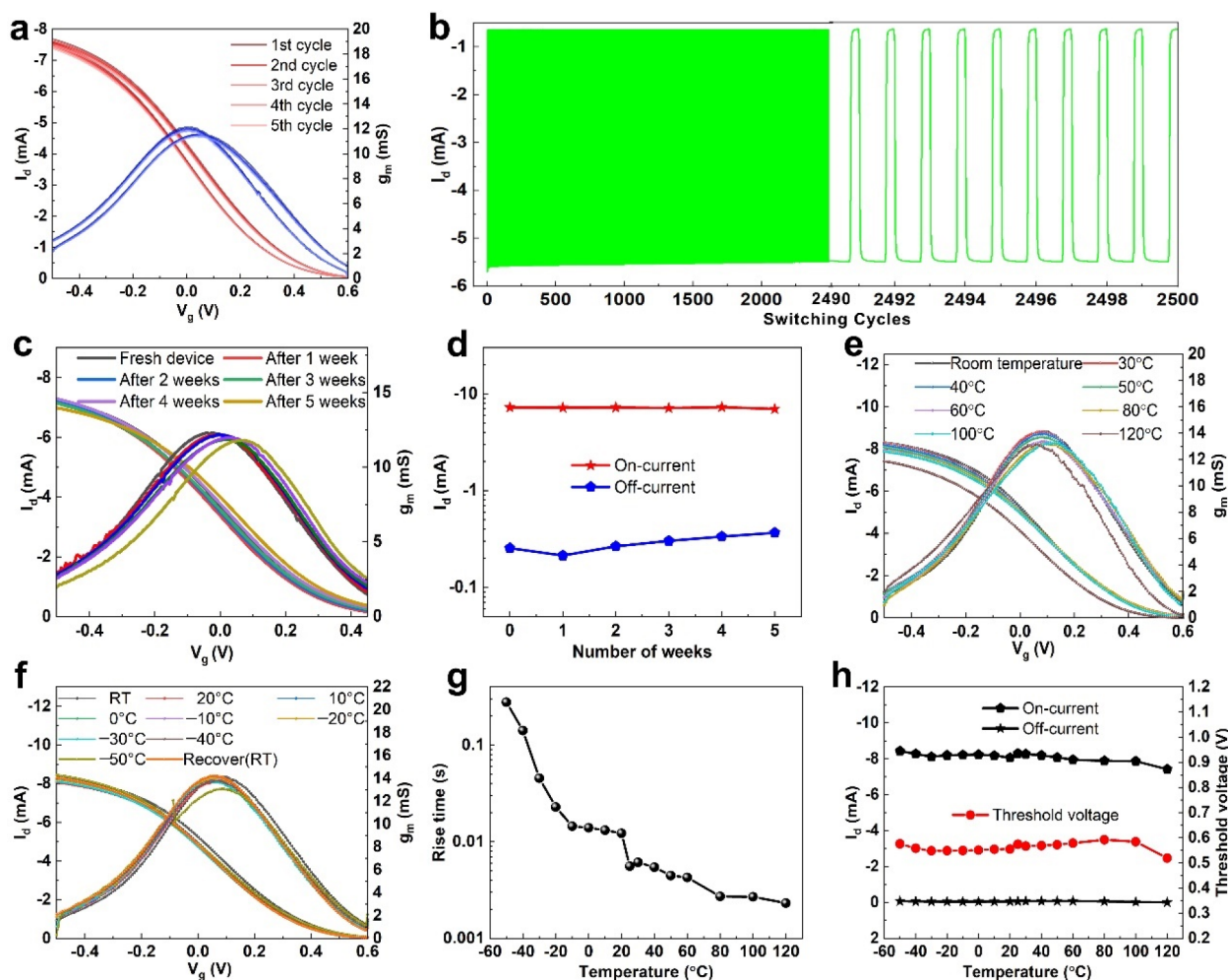


Figure 4. Characterizations of PEDOT:PSS-based SSOECT in terms of electrical stability, long-term stability, and temperature resilience. 50% weight EMIM:BF₄ was blended with the TPU polymer as a solid electrolyte. (a) Five continuous DC cycles of double-sweep transfer curves. (b) Pulsing endurance of SSOECT, 98.6% I_{on} was maintained after 2500 switching cycles with 0.4 V, 50 ms/−0.2 V 150 ms pulse/base value. (c) Weekly measured transfer curves and transconductances of SSOECT. (d) On and off current (I_{off}) of SSOECT over 5 weeks, kept in air ambient conditions. (e) Transfer curves of SSOECT operated at high-temperature range from RT to 120 °C. (f) Transfer curves of SSOECT operated in a low-temperature range from RT to −50 °C. (g) Rise time variation under a temperature range from −50 to 120 °C. (h) Summary of I_{on} , I_{off} , and threshold voltage under the temperature range from −50 to 120 °C.

first to fifth cycles perform negligible cycle-to-cycle variations regarding I_{on} and transconductance. After that, the same channel went through 2500 switching cycles, and an excellent cycling endurance was obtained with 98.6% of current retention, shown in Figure 4b. Subsequently, the device was kept in ambient air and measured weekly, where the transfer characteristics in 5 weeks are shown in Figure 4c. Nearly 96.6% of I_{on} was maintained after 5 weeks, shown in Figure 4d. The cycling endurance of SSOECTs using other semiconductors and ion sources are also shown in Figure S19.

Stable and efficient operation of OECT at low and high temperatures is helpful for its functional evaluation under extreme conditions, e.g., high-power computers, desert expeditions, and space exploration. Figure 4e and f show the transfer curves of the SSOECT in two temperature regimes, one at higher temperatures (23 to 120 °C) and another one at a lower temperature (−50 to 23 °C). Nearly 94.8% of the current value was retained while increasing the temperature from 23 to 100 °C, and the transistor could even switch at 120 °C, which is the highest reported operating temperature for OECTs.^{20,22} The response time of the SSOECTs is highly

temperature-dependent since the ionic conductivity and ion motion exhibit a positive proportion with temperature. Temperature increases from −50 to 120 °C could improve the response speed from 277 to 2.32 ms (Figure 4g), since the ion movement was suppressed at low temperatures and excited at high temperatures. Our SSOECTs using TPU-based solid electrolytes are found to operate stably from −50 °C to above 100 °C, which meets the temperature range requirements in most electronic applications. Notably, the SSOECT working at −40 °C showed good device stability over prolonged cycling where the drain current retained 98.2% of the original value after 1000 cycles (Figure S20). The threshold voltage shift is also negligible, within 0.1 V, shown in Figure 4h.

Because of the high elasticity of TPU-based ionic gel, we also fabricated flexible SSOECTs on a polyethylene terephthalate (PET) substrate (Figure 5a).^{39,40} First, the transfer curve of the transistor was obtained and compared with the same W/L channel on a rigid Si/SiO₂ substrate. Both flexible and rigid devices showed similar performance in terms of I_{on} (~4.6 mA for flexible, 4.1 mA for rigid substrate) and peak g_m (8.55 mS for flexible, 7.96 mS for rigid), as shown in Figure 5b.

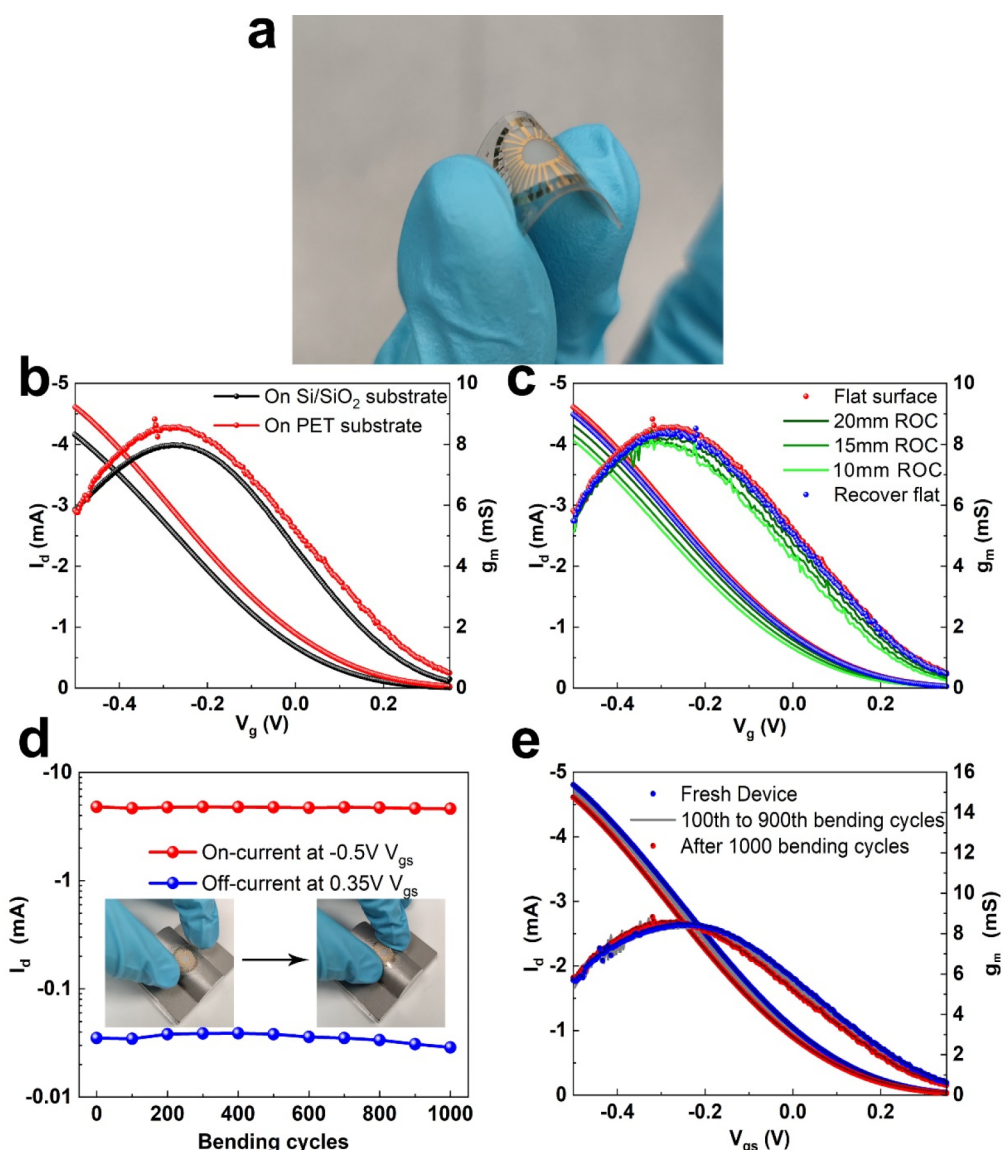


Figure 5. Application of our SSOECT for flexible electronics. 50% weight EMIM:BF₄ was blended with a TPU polymer as a solid electrolyte for the PEDOT:PSS system. All of the data were obtained from $W/L = 100 \mu\text{m}/20 \mu\text{m}$ channels. (a) Image of flexible SSOECTs on the PET substrate. (b) Comparison of SSOECT's performance on a flexible substrate and a rigid substrate. (c) Transfer curves of fresh OECT, bent in 20 mm, 15 mm, and 10 mm ROC, and recover to a flat surface. (d) The change in $I_{\text{on}}/I_{\text{off}}$ of SSOECT, before and after bending 1000 cycles. (e) Transfer curves of SSOECT, before and after bending 1000 cycles.

Flexibility of SSOECT was evaluated by placing the device on a curved surface and varying the bending radius (ROCs = 20, 15, 10 mm), as shown in the inset image of Figure 5d. Stable OECT performance was maintained, with high retention of the I_{on} (>90%) and corresponding peak transconductance (>94%) even after being bent at an ROC as low as 10 mm (Figure 5c). Importantly, the current almost fully recovered after putting the flexible device on the flat surface again. Afterward, the substrate was placed on the bending stage with a 10 mm ROC and bent uninterruptedly for 1000 cycles, and the transfer curves of OECT were measured after every 100 bending cycles. Nearly 96% I_{on} was retained after 1000 bending cycles, while I_{off} presented a slight decrease (Figure 5d and e).

OECTs have been used as local transducers of bioelectronic signals, while their measured current signal output presents challenges for practical implementation. Since the electrochemical doping of conjugated semiconductors can be

triggered at a low bias (<1 V), the OECT-based circuit allows a much lower supply voltage (V_{dd}) and subsequently offers new opportunities for high-performance signal processing. In this work, we implement three different designs of inverter circuits based on our SSOECTs. For easy integration, the same TPU polymer electrolyte was utilized for all semiconductor channels (50% weight EMIM:TFSI in TPU polymer). First, a unipolar inverter was constructed with a P3HT-based transistor and a resistor (Figure 6a). The transfer curves and voltage gains of such an inverter under varying V_{dd} are presented in Figure 6b, where TFSI⁻ in a TPU electrolyte will dope the P3HT channel under a negative input gate bias (V_{in}), and subsequently output voltage (V_{out}) drops to 0 V. A gain value ($G = \partial V_{\text{out}}/\partial V_{\text{in}}$) of ~ 10 was achieved at $-0.85 \text{ V } V_{\text{dd}}$. Next, to improve the tuning efficiency, the resistor was replaced by a feedback transistor (PEDOT:PSS based), where the gate was directly connected to the output (Figure 6c). A gain of ~ 24 was obtained (at V_{dd}

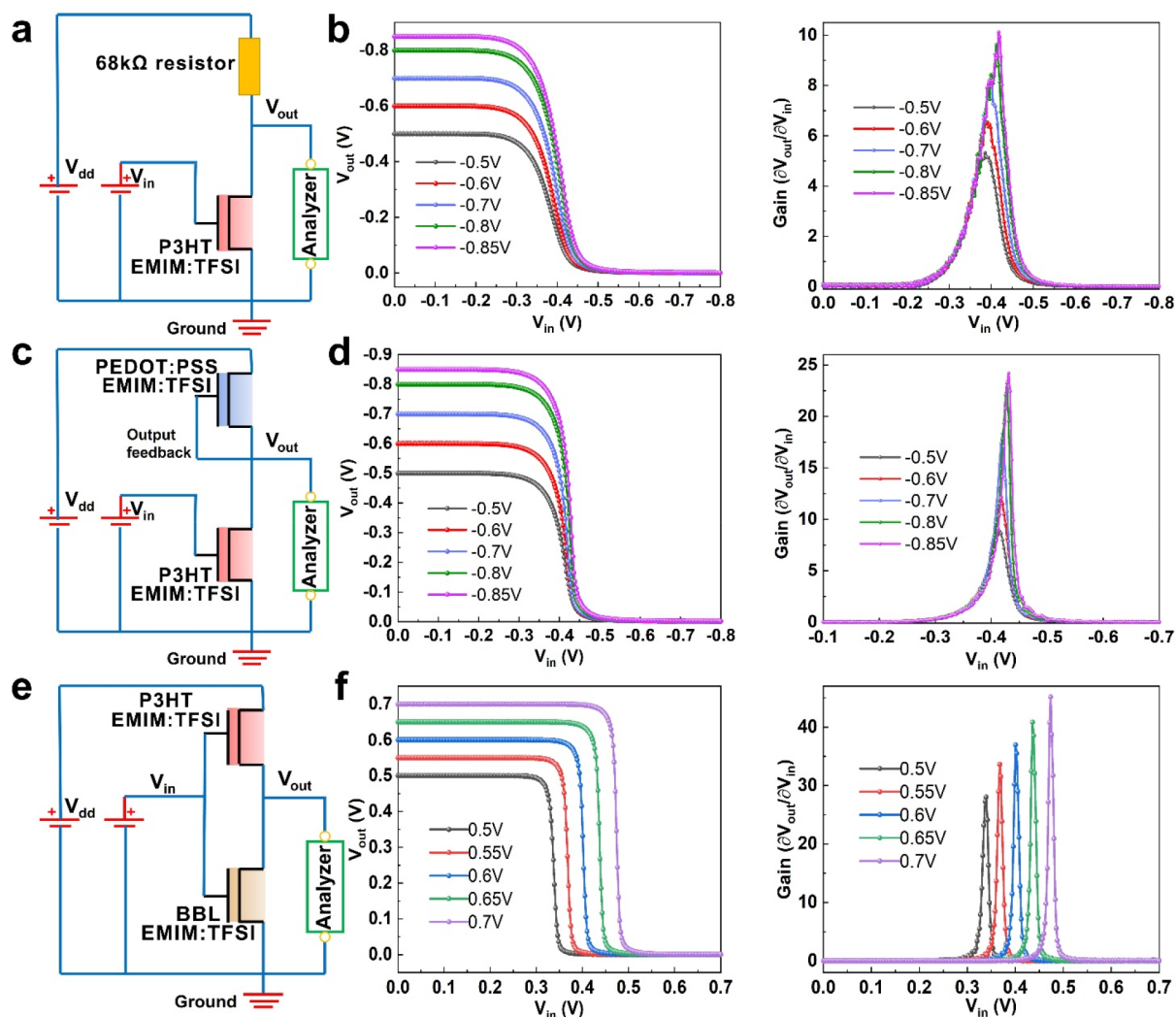


Figure 6. Application of our SSOECT for the inverter circuit. 50% weight EMIM:TFSI was blended with TPU polymer as a solid electrolyte for both p and n-type channels for ease of integration. $W/L = 10 \mu\text{m}/20 \mu\text{m}$ for PEDOT:PSS-based SSOECT, while $W/L = 100 \mu\text{m}/10 \mu\text{m}$ for P3HT and BBL-based SSOECTs. (a) Circuit schematic of unipolar inverter built up by a p-type SSOECT and resistor. (b) Transfer curves and gain of inverter based on p-type SSOECT and resistor. (c) Circuit schematic of unipolar inverter built up by two p-type SSOECTs. (d) Transfer curves and gain of inverter-based on two p-type SSOECTs. (e) Circuit schematic of complementary inverter built up by n- and p-type SSOECTs. (f) Transfer curves and gain of inverter-based on n- and p-type SSOECTs.

$= -0.85 \text{ V}$), and the channel conductance of the feedback transistor is proportional to the output, allowing a more effective tuning of V_{out} (Figure 6d).

Compared with unipolar inverters, a complementary inverter consisting of n-type and p-type OECTs can achieve faster transition of V_{out} and higher voltage gain.^{59,60} Hence, we constructed an all-solid-state complementary inverter based on SSOECTs using P3HT and BBL as p-type and n-type organic semiconductors, respectively (Figure 6e), where the detailed transfer performance of each elementary transistor is shown in Figure S21. This complementary inverter could be operated under low supply voltage (from 0.5 to 0.7 V). A 0.22 V noise margin was obtained under 0.7 V V_{dd} , which reached 63% of the theoretical value ($V_{\text{dd}}/2 = 0.35 \text{ V}$). Notably, the voltage gain of such a SSOECT-based inverter could reach 46 under a 0.7 V supply voltage (Figure 6f), which is much higher than previous unipolar inverters and most of the reported OECT-based inverters as shown in Table S3.^{61–64} Moreover, the transient response was also improved significantly for such a complementary structure, where the rise and fall time of V_{out}

were calculated as 0.028 and 0.34 s, respectively, 10 times faster than unipolar inverters (Figure S23).

3. CONCLUSION

In conclusion, a TPU polymer matrix was first explored as a solid electrolyte for OECT devices. Four conjugated semiconductors (PEDOT:PSS, P3HT, PCDTFBT, BBL) and three types of ionic liquids (EMIM:TFSI, EMIM:BF₄, EMIM:OTF) were induced and investigated. The results demonstrated that the solid electrolyte is a versatile choice to construct highly performing and stable OECTs with excellent cycling endurance (98.6% data retention after 2500 cycles), good long-term stability (96.6% data retention after 5 weeks in ambient conditions), and thermal stability up to 120 °C. A negligible change in $I_{\text{on}}/I_{\text{off}}$ and V_{th} in the temperature range of -50 to $100 \text{ }^\circ\text{C}$ is observed. The development of SSOECTs capable of functioning over low- and high-temperature environments will further expand their applications, such as in high-power computers, desert expeditions, and space

exploration. Additionally, due to the high elasticity of TPU-based films, flexible SSOECTs were demonstrated and went through the bending measurement in varying ROCs and bending cycles, presenting their potential for flexible and wearable sensor applications. Finally, three types of SSOECT-based inverters were fabricated in unipolar and complementary configurations. The complementary inverter presented a lower supply voltage, faster response, and higher gain (46) as compared with the unipolar inverters. Overall, these results emphasize the great potential of TPU-based ionic gel as a solid electrolyte that enables robust OECT devices toward flexible electronics and bioelectronics.

EXPERIMENTAL SECTION

Materials. Poly(3,4-ethylenedioxythiophene):poly(styrenesulfonate) (PEDOT:PSS, Clevis PH1000) was purchased from Heraeus. Poly(3-hexythiophene-2,5-diyl) (P3HT), poly[(5-fluoro-2,1,3-benzothiadiazole-4,7-diyl)(4,4-dihexadecyl-4H-cyclopenta[2,1-b:3,4-b'] dithiophene-2,6-diyl)(6-fluoro-2,1,3-benzothiadiazole-4,7-diyl)(4,4-dihexadecyl-4H-cyclopenta[2,1-b:3,4-b']-dithiophene-2,6-diyl)] (PCDTFBT), thermoplastic polyurethane (TPU), 1-ethyl-3-methylimidazolium bis(trifluoromethylsulfonyl)amide (EMIM:TFSI), 1-ethyl-3-methylimidazolium trifluoromethanesulfonate (EMIM:OTF), 1-ethyl-3-methylimidazolium tetrafluoroborate (EMIM:BF₄), and all of the processing solvents including acetone, dimethylformamide, chloroform, and ethanol were all obtained from Sigma-Aldrich and used as received. The BBL was synthesized according to the reported literature.^{65,66}

Fabrication of SPE Film. First, a 2 g thermoplastic polyurethane pellet was dissolved in 4 mL of acetone and 4 mL of dimethylformamide cosolvent and followed by vigorous stirring at 100 °C for 6 h until all pellets dissolved. Then, the ionic liquids were added to the above solution with varying weight ratios and followed by vigorous vibration for 30 min. After removing bubbles in the solution by standing still, the prepared solution was poured into a Petri dish and annealed inside a vacuum oven at 120 °C for more than 24 h. A 10 wt % electrolyte film comprised 10 wt % of the ionic liquid and 90 wt % of the TPU polymer, while 30 and 50 wt % electrolyte film comprised 30 wt % and 50 wt % of ionic liquid and 70 wt % and 50 wt % of TPU polymer, respectively. Finally, the formed free-standing film was peeled off and cut into small pieces and clamped by two stainless steel sheets for ionic conductivity measurement. The measurement was done at 25 °C at a 70% humidity level.

Fabrication of SSOECTs. First, the Si/SiO₂ wafer was cleaned with acetone and ethanol for 5 min each under ultrasonic conditions. AZ5214E photoresist was used for source/drain patterning, which was spin-coated on top of the precleaned substrates and exposed to UV light using a SUSS MJB4 mask aligner, and then developed by AZ developer. Thereafter, 50 nm of gold with 5 nm of titanium as a seed layer was evaporated on the substrate sequentially via E-beam evaporation, followed by lift-off of the photoresist by immersion of the substrates in acetone for 10 min with sonication. Then, a 2- μ m-thick Parylene C layer with an adhesion promoter of 3(trimethoxysilyl)propyl methacrylate (A-174 Silane) was deposited to insulate the contacts from the electrolyte using SCS Labcoater. An antiadhesion layer of dilute cleaner (Micro-90, 10 wt % in deionized water) was spin-coated to facilitate the peel-off procedure. After that, a second Parylene-C layer (~2.5 μ m) was deposited, acting as a sacrificial layer. A second lithography process was conducted on the substrates to expose the channel and contact pad area, where AZ4620 and AZ351B were used as the photoresist and developer, respectively. The patterned channel area and contact pads were etched via reactive ion etching (Oxford Plasmalab80) at 50 sccm O₂, 10 sccm CHF₃, and 160 W operating conditions. PEDOT:PSS, Clevis PH1000, 5 mg mL⁻¹ P3HT, and PCDTFBT dissolved in chloroform were spin-coated on the prepared substrate followed by peeling-off of the second layer of parylene. BBL was prepared in a methanesulfonic acid (MSA) solution at a concentration of 5 mg mL⁻¹. After spin-coating, the BBL

films were immersed in DI water for 15 min to remove the MSA in the film, followed by peeling-off of the second layer of parylene and annealed at 200 °C for 1 h in a N₂ filled glovebox. Solid electrolyte solution was directly spin-coated on top of the channel at 500 rpm for 60 s, which is followed by drying in a vacuum chamber for more than 24 h. The resulting electrolyte films are measured to be 10.93 μ m, 9.04 μ m, and 6.55 μ m for EMIM:BF₄, EMIM:OTF, and EMIM:TFSI, respectively, using a surface profiler.

Electrical Characterizations. Solid electrolyte was covered by a polyimide film coated with Au/PEDOT:PSS as the gate electrode. The *I*-*V* characteristics of the films and all of the OECT device characteristics, including output and transfer curves and pulse measurement, were measured under ambient conditions using Keysight precision source/measure unit (B2912A) and a probe station (Karl Suss PMS). Scan rate was kept at 25 mV s⁻¹ for DC. Electrochemical impedance spectroscopy (EIS) was employed to check the volumetric capacitance of the PEDOT:PSS films using the Metrohm Autolab system. For ionic conductivity measurement, the metal-insulator-metal (MIM) structure was formed by two pieces of stainless steel separated by the SPE film. The input signal was a sine wave (amplitude of 10 mV) with a frequency range from 10 000 to 1 Hz. For bending measurements, because of the small radius of curvatures (ROCs) applied to substrates, the gate electrode of the Au/PEDOT coated PI film was challenging to attach conformably to the electrolyte. Hence, a Ag/AgCl pellet was directly in contact with SPE as the gate electrode. The detailed *V*_{th} extraction method is shown in Figure S22.

Electrochemistry Spectroscopy. The PEDOT:PSS solution was spin-coated on ITO glass substrates in the air and subsequently annealed at 140 °C for 20 min. The P3HT and PCDTFBT film on ITO glass was prepared in a glovebox. Then, the solid electrolyte was spin-coated onto the ITO glass to cover the PEDOT:PSS or P3HT, PCDTFBT films, followed by the encapsulation of another ITO glass which can act as the gate electrode. A Keysight precision source/measure unit (B2912A) was chosen to apply biasing between the gate electrode and ITO glass. The absorption spectra were recorded using a UV-vis-NIR spectrophotometer (SHIMADZU, UV-3600) over the wavelength range from 350 to 1250 nm as the sample was biased. Another sample without the semiconductor layer was used to get the baseline.

ASSOCIATED CONTENT

Supporting Information

The Supporting Information is available free of charge at <https://pubs.acs.org/doi/10.1021/acsaelm.3c00091>.

SEM of electrolyte films, detailed transfer/output, cycling stability of transistors, statistical studies of transistors performance, inverter performance, transistor/inverter performance comparison tables, additional temperature studies, *V*_{th} extraction method (PDF)

AUTHOR INFORMATION

Corresponding Authors

Wen Siang Lew – School of Physical and Mathematical Sciences, Nanyang Technological University, Singapore 637371, Singapore; orcid.org/0000-0002-5161-741X; Email: wensiang@ntu.edu.sg

Wei Lin Leong – School of Electrical and Electronic Engineering, Nanyang Technological University, Singapore 639798, Singapore; orcid.org/0000-0002-1402-0083; Email: wleong@ntu.edu.sg

Authors

Kunqi Hou – School of Physical and Mathematical Sciences, Nanyang Technological University, Singapore 637371, Singapore

Shuai Chen – School of Electrical and Electronic Engineering, Nanyang Technological University, Singapore 639798, Singapore

Akshay Moudgil – School of Electrical and Electronic Engineering, Nanyang Technological University, Singapore 639798, Singapore; orcid.org/0000-0002-7758-5436

Xihu Wu – School of Electrical and Electronic Engineering, Nanyang Technological University, Singapore 639798, Singapore

Teck Lip Dexter Tam – Institute of Sustainability for Chemical, Engineering and Environment (ISCE2), Agency of Science, Technology and Research (A*STAR), Singapore 627833, Singapore; orcid.org/0000-0003-2423-4752

Complete contact information is available at:
<https://pubs.acs.org/10.1021/acsaelm.3c00091>

Notes

The authors declare no competing financial interest.

ACKNOWLEDGMENTS

W.L.L. would like to acknowledge funding support from the Delta-NTU Corporate Lab through the A*STAR IAF-ICP (No. I2201E0013) and Ministry of Education (MOE) under an AcRF Tier 2 Grant (2019-T2-2-106). This work is also supported by an A*STAR AME IAF-ICP (No. I1801E0030) grant.

REFERENCES

- Berggren, M.; Simon, D. T.; Nilsson, D.; Dyreklev, P.; Norberg, P.; Nordlinder, S.; Ersman, P. A.; Gustafsson, G.; Wikner, J. J.; Hederen, J.; Hentzell, H. Browsing the real world using organic electronics, Si-chips, and a human touch. *Adv. Mater.* **2016**, *28* (10), 1911–1916.
- Wu, X.; Surendran, A.; Ko, J.; Filonik, O.; Herzig, E. M.; Müller-Buschbaum, P.; Leong, W. L. Ionic-liquid doping enables high transconductance, fast response time, and high ion sensitivity in organic electrochemical transistors. *Adv. Mater.* **2019**, *31* (2), 1805544.
- Rivnay, J.; Owens, R. i. M.; Malliaras, G. G. The rise of organic bioelectronics. *Chem. Mater.* **2014**, *26* (1), 679–685.
- Someya, T.; Bao, Z.; Malliaras, G. G. The rise of plastic bioelectronics. *Nature* **2016**, *540* (7633), 379–385.
- Hamed, M.; Forchheimer, R.; Inganäs, O. Towards woven logic from organic electronic fibres. *Nature materials* **2007**, *6* (5), 357–362.
- van de Burgt, Y.; Lubberman, E.; Fuller, E. J.; Keene, S. T.; Faria, G. C.; Agarwal, S.; Marinella, M. J.; Talin, A. A.; Salleo, A. A non-volatile organic electrochemical device as a low-voltage artificial synapse for neuromorphic computing. *Nature materials* **2017**, *16* (4), 414–418.
- Rivnay, J.; Inal, S.; Salleo, A.; Owens, R. M.; Berggren, M.; Malliaras, G. G. Organic electrochemical transistors. *Nature Reviews Materials* **2018**, *3* (2), 17086.
- Rivnay, J.; Leleux, P.; Ferro, M.; Sessolo, M.; Williamson, A.; Koutsouras, D. A.; Khodagholy, D.; Ramuz, M.; Strakosas, X.; Owens, R. M.; Benar, C.; Badier, J. M.; Bernard, C.; Malliaras, G. G. High-performance transistors for bioelectronics through tuning of channel thickness. *Science Advances* **2015**, *1* (4), e1400251.
- Khodagholy, D.; Rivnay, J.; Sessolo, M.; Gurfinkel, M.; Leleux, P.; Jimison, L. H.; Stavrinidou, E.; Herve, T.; Sanaur, S.; Owens, R. M.; Malliaras, G. G. High transconductance organic electrochemical transistors. *Nat. Commun.* **2013**, *4*, 2133.
- Spyropoulos, G. D.; Gelinas, J. N.; Khodagholy, D. Internal ion-gated organic electrochemical transistor: A building block for integrated bioelectronics. *Science Advances* **2019**, *5* (2), eaau7378.
- Ohayon, D.; Nikiforidis, G.; Savva, A.; Giugni, A.; Wustoni, S.; Palanisamy, T.; Chen, X.; Maria, I. P.; Di Fabrizio, E.; Costa, P.; McCulloch, I.; Inal, S. Biofuel powered glucose detection in bodily fluids with an n-type conjugated polymer. *Nat. Mater.* **2020**, *19*, 456–463.
- Lee, W.; Kobayashi, S.; Nagase, M.; Jimbo, Y.; Saito, I.; Inoue, Y.; Yambe, T.; Sekino, M.; Malliaras, G. G.; Yokota, T.; Tanaka, M.; Someya, T. Nonthrombogenic, stretchable, active multielectrode array for electroanatomical mapping. *Science Advances* **2018**, *4* (10), eaau2426.
- Lee, W.; Kim, D.; Rivnay, J.; Matsuhisa, N.; Lonjaret, T.; Yokota, T.; Yawo, H.; Sekino, M.; Malliaras, G. G.; Someya, T. Integration of organic electrochemical and field-effect transistors for ultraflexible, high temporal resolution electrophysiology arrays. *Adv. Mater.* **2016**, *28* (44), 9722–9728.
- Chen, S.; Surendran, A.; Wu, X.; Leong, W. L. Contact Modulated Ionic Transfer Doping in All-Solid-State Organic Electrochemical Transistor for Ultra-High Sensitive Tactile Perception at Low Operating Voltage. *Adv. Funct. Mater.* **2020**, *30*, 2006186.
- Surendran, A.; Chen, S.; Lew, J. H.; Wu, X.; Koh, T. M.; Leong, W. L. Self-Powered Organic Electrochemical Transistors with Stable, Light-Intensity Independent Operation Enabled by Carbon-Based Perovskite Solar Cells. *Advanced Materials Technologies* **2021**, *6*, 2100565.
- Andersson Ersman, P.; Nilsson, D.; Kawahara, J.; Gustafsson, G.; Berggren, M. Fast-switching all-printed organic electrochemical transistors. *Org. Electron.* **2013**, *14* (5), 1276–1280.
- Yang, C.-Y.; Tu, D.; Ruoko, T.-P.; Gerasimov, J. Y.; Wu, H.-Y.; Harikesh, P. C.; Massetti, M.; Stoeckel, M.-A.; Kroon, R.; Muller, C.; Berggren, M.; Fabiano, S. Low-power/high-gain flexible complementary circuits based on printed organic electrochemical transistors. *Adv. Electron. Mater.* **2022**, *8*, 2100907.
- Quill, T. J.; LeCroy, G.; Melianas, A.; Rawlings, D.; Thiburce, Q.; Sheelamantula, R.; Cheng, C.; Tuchman, Y.; Keene, S. T.; McCulloch, I.; Segalman, R. A.; Chabiny, M. L.; Salleo, A. Ion Pair Uptake in Ion Gel Devices Based on Organic Mixed Ionic–Electronic Conductors. *Adv. Funct. Mater.* **2021**, *31* (47), 2104301.
- Kim, D.; Jang, H.; Lee, S.; Kim, B. J.; Kim, F. S. Solid-State Organic Electrolyte-Gated Transistors Based on Doping-Controlled Polymer Composites with a Confined Two-Dimensional Channel in Dry Conditions. *ACS Appl. Mater. Interfaces* **2021**, *13* (1), 1065–1075.
- Melianas, A.; Quill, T. J.; LeCroy, G.; Tuchman, Y.; Loo, H. v.; Keene, S. T.; Giovannitti, A.; Lee, H. R.; Maria, I. P.; McCulloch, I.; Salleo, A. Temperature-resilient solid-state organic artificial synapses for neuromorphic computing. *Science Advances* **2020**, *6* (27), eabb2958.
- Cho, K. G.; Cho, Y. K.; Kim, J. H.; Yoo, H. Y.; Hong, K.; Lee, K. H. Thermostable Ion Gels for High-Temperature Operation of Electrolyte-Gated Transistors. *ACS Appl. Mater. Interfaces* **2020**, *12* (13), 15464–15471.
- Han, S.; Yu, S.; Hu, S.; Chen, H.-j.; Wu, J.; Liu, C. A high endurance, temperature-resilient, and robust organic electrochemical transistor for neuromorphic circuits. *Journal of Materials Chemistry C* **2021**, *9* (35), 11801–11808.
- Wang, S.; Min, K. Solid polymer electrolytes of blends of polyurethane and polyether modified polysiloxane and their ionic conductivity. *Polymer* **2010**, *51* (12), 2621–2628.
- Tao, C.; Gao, M.-H.; Yin, B.-H.; Li, B.; Huang, Y.-P.; Xu, G.; Bao, J.-J. A promising TPU/PEO blend polymer electrolyte for all-solid-state lithium ion batteries. *Electrochim. Acta* **2017**, *257*, 31–39.
- Jiang, Y.; Li, F.; Mei, Y.; Ding, Y.; Pang, H.; Zhang, P. Gel polymer electrolyte based on hydrophilic–lipophilic TiO₂-modified thermoplastic polyurethane for high-performance Li-ion batteries. *J. Mater. Sci.* **2021**, *56* (3), 2474–2485.
- Hwang, H. J.; Kim, J. S.; Kim, W.; Park, H.; Bhatia, D.; Jee, E.; Chung, Y. S.; Kim, D. H.; Choi, D. An Ultra-Mechanosensitive Visco-Poroelastic Triboelectric Ion Pump for Continuous Self-Powering Kinematic Triboelectric Nanogenerators. *Adv. Energy Mater.* **2019**, *9* (17), 1803786.

- (27) Ramanjaneyulu, K.; Bar, N.; Arif Sher Shah, M. S.; Manorama, S. V.; Basak, P. Semi-interpenetrating polymer networks as solid polymer electrolytes: Effects of ion-dissociation, crosslink density and oligomeric entanglements on the conductivity behavior in poly (ethylene oxide)–polyurethane/poly (acrylonitrile) matrix. *J. Power Sources* **2012**, *217*, 29–36.
- (28) Wu, N.; Cao, Q.; Wang, X.; Chen, Q. Study of a novel porous gel polymer electrolyte based on TPU/PVdF by electrospinning technique. *Solid State Ionics* **2011**, *203* (1), 42–46.
- (29) Park, D. H.; Park, H. W.; Chung, J. W.; Nam, K.; Choi, S.; Chung, Y. S.; Hwang, H.; Kim, B.; Kim, D. H. Highly Stretchable, High-Mobility, Free-Standing All-Organic Transistors Modulated by Solid-State Elastomer Electrolytes. *Adv. Funct. Mater.* **2019**, *29* (18), 1808909.
- (30) Lieberth, K.; Brückner, M.; Torricelli, F.; Mailänder, V.; Gkoupidenis, P.; Blom, P. W. Monitoring Reversible Tight Junction Modulation with a Current-Driven Organic Electrochemical Transistor. *Advanced Materials Technologies* **2021**, *6* (5), 2000940.
- (31) Tarabella, G.; Vurro, D.; Lai, S.; D'Angelo, P.; Ascari, L.; Iannotta, S. Aerosol jet printing of PEDOT:PSS for large area flexible electronics. *Flexible and Printed Electronics* **2020**, *5* (1), 014005.
- (32) D'Angelo, P.; Tarabella, G.; Romeo, A.; Marasso, S. L.; Verna, A.; Cocuzza, M.; Peruzzi, C.; Vurro, D.; Iannotta, S. PEDOT: PSS morphostructure and ion-to-electron transduction and amplification mechanisms in organic electrochemical transistors. *Materials* **2019**, *12* (1), 9.
- (33) Massaglia, G.; Chiodoni, A.; Marasso, S.; Pirri, C.; Quaglio, M. Electrical conductivity modulation of crosslinked composite nanofibers based on PEO and PEDOT: PSS. *J. Nanomater.* **2018**, *2018*, 1–7.
- (34) Wen, T.-C.; Luo, S.-S.; Yang, C.-H. Ionic conductivity of polymer electrolytes derived from various diisocyanate-based waterborne polyurethanes. *Polymer* **2000**, *41* (18), 6755–6764.
- (35) Chen, W. C.; Chen, H. H.; Wen, T. C.; Digar, M.; Gopalan, A. Morphology and ionic conductivity of thermoplastic polyurethane electrolytes. *J. Appl. Polym. Sci.* **2004**, *91* (2), 1154–1167.
- (36) Tian, L. y.; Zhu, W. h.; Tang, X. Polymer gel electrolytes based on thermoplastic polyurethane. *J. Appl. Polym. Sci.* **2003**, *90* (9), 2310–2315.
- (37) Liu, X.; Song, K.; Lu, C.; Huang, Y.; Duan, X.; Li, S.; Ding, Y. Electrospun PU@GO separators for advanced lithium ion batteries. *J. Membr. Sci.* **2018**, *555*, 1–6.
- (38) Cai, M.; Zhu, J.; Yang, C.; Gao, R.; Shi, C.; Zhao, J. A parallel bicomponent TPU/PI membrane with mechanical strength enhanced isotropic interfaces used as polymer electrolyte for lithium-ion battery. *Polymers* **2019**, *11* (1), 185.
- (39) Jin, M. L.; Park, S.; Kim, J. S.; Kwon, S. H.; Zhang, S.; Yoo, M. S.; Jang, S.; Koh, H. J.; Cho, S. Y.; Kim, S. Y.; Ahn, C. W.; Cho, K.; Lee, S. G.; Kim, D. H.; Jung, H. T. An Ultrastable Ionic Chemiresistor Skin with an Intrinsically Stretchable Polymer Electrolyte. *Adv. Mater.* **2018**, *30* (20), 1706851.
- (40) Ye, F.; Zhang, X.; Liao, K.; Lu, Q.; Zou, X.; Ran, R.; Zhou, W.; Zhong, Y.; Shao, Z. A smart lithiophilic polymer filler in gel polymer electrolyte enables stable and dendrite-free Li metal anode. *Journal of Materials Chemistry A* **2020**, *8* (19), 9733–9742.
- (41) Weissbach, A.; Bongartz, L. M.; Cucchi, M.; Tseng, H.; Leo, K.; Kleemann, H. Photopatternable solid electrolyte for integrable organic electrochemical transistors: operation and hysteresis. *Journal of Materials Chemistry C* **2022**, *10*, 2656–2662.
- (42) Mackanic, D. G.; Yan, X.; Zhang, Q.; Matsuhisa, N.; Yu, Z.; Jiang, Y.; Manika, T.; Lopez, J.; Yan, H.; Liu, K.; Chen, X.; Cui, Y.; Bao, Z. Decoupling of mechanical properties and ionic conductivity in supramolecular lithium ion conductors. *Nat. Commun.* **2019**, *10* (1), 5384.
- (43) Bérardan, D.; Franger, S.; Meena, A.; Drago, N. Room temperature lithium superionic conductivity in high entropy oxides. *Journal of Materials Chemistry A* **2016**, *4* (24), 9536–9541.
- (44) Deng, Y.; Eames, C.; Fleutot, B.; David, R.; Chotard, J.-N.; Suard, E.; Masquelier, C.; Islam, M. S. Enhancing the lithium ion conductivity in lithium superionic conductor (LISICON) solid electrolytes through a mixed polyanion effect. *ACS Appl. Mater. Interfaces* **2017**, *9* (8), 7050–7058.
- (45) Verma, A.; Stoppelman, J. P.; McDaniel, J. G. Tuning Water Networks via Ionic Liquid/Water Mixtures. *International journal of molecular sciences* **2020**, *21* (2), 403.
- (46) Ho, T. D.; Zhang, C.; Hantao, L. W.; Anderson, J. L. Ionic liquids in analytical chemistry: fundamentals, advances, and perspectives. *Analytical chemistry* **2014**, *86* (1), 262–285.
- (47) Kawano, R.; Matsui, H.; Matsuyama, C.; Sato, A.; Susan, M. A. B. H.; Tanabe, N.; Watanabe, M. High performance dye-sensitized solar cells using ionic liquids as their electrolytes. *J. Photochem. Photobiol., A* **2004**, *164* (1–3), 87–92.
- (48) Wu, X.; Stephen, M.; Hidalgo, T. C.; Salim, T.; Surgailis, J.; Surendran, A.; Su, X.; Li, T.; Inal, S.; Leong, W. L. Ionic-Liquid Induced Morphology Tuning of PEDOT: PSS for High-Performance Organic Electrochemical Transistors. *Adv. Funct. Mater.* **2022**, *32* (1), 2108510.
- (49) Li, Q.; Yang, J.; Chen, S.; Zou, J.; Xie, W.; Zeng, X. Highly conductive PEDOT:PSS transparent hole transporting layer with solvent treatment for high performance silicon/organic hybrid solar cells. *Nanoscale Res. Lett.* **2017**, *12* (1), 1–8.
- (50) Dong, J.; Portale, G. Role of the Processing Solvent on the Electrical Conductivity of PEDOT: PSS. *Advanced Materials Interfaces* **2020**, *7* (18), 2000641.
- (51) Oh, S. H.; Heo, S. J.; Yang, J. S.; Kim, H. J. Effects of ZnO nanoparticles on P3HT: PCBM organic solar cells with DMF-modulated PEDOT: PSS buffer layers. *ACS Appl. Mater. Interfaces* **2013**, *5* (22), 11530–11534.
- (52) Zhang, S.; Fan, Z.; Wang, X.; Zhang, Z.; Ouyang, J. Enhancement of the thermoelectric properties of PEDOT: PSS via one-step treatment with cosolvents or their solutions of organic salts. *Journal of Materials Chemistry A* **2018**, *6* (16), 7080–7087.
- (53) Yan, Y.; Wu, X.; Chen, Q.; Liu, Y.; Chen, H.; Guo, T. High-Performance Low-Voltage Flexible Photodetector Arrays Based on All-Solid-State Organic Electrochemical Transistors for Photosensing and Imaging. *ACS Appl. Mater. Interfaces* **2019**, *11* (22), 20214–20224.
- (54) Nguyen-Dang, T.; Harrison, K.; Lill, A.; Dixon, A.; Lewis, E.; Vollbrecht, J.; Hachisu, T.; Biswas, S.; Visell, Y.; Nguyen, T. Q. Biomaterial-Based Solid-Electrolyte Organic Electrochemical Transistors for Electronic and Neuromorphic Applications. *Advanced Electronic Materials* **2021**, *7* (12), 2100519.
- (55) Bi, S.; Wang, R.; Liu, S.; Yan, J.; Mao, B.; Kornyshev, A. A.; Feng, G. Minimizing the electrosorption of water from humid ionic liquids on electrodes. *Nat. Commun.* **2018**, *9* (1), 1–9.
- (56) de Izarra, A.; Choi, C.; Jang, Y. H.; Lansac, Y. Ionic Liquid for PEDOT: PSS Treatment. Ion Binding Free Energy in Water Revealing the Importance of Anion Hydrophobicity. *J. Phys. Chem. B* **2021**, *125* (7), 1916–1923.
- (57) Zhang, L.; Deng, H.; Liu, S.; Zhang, Q.; Chen, F.; Fu, Q. Enhanced thermoelectric properties of PEDOT: PSS films via a novel two-step treatment. *RSC Adv.* **2015**, *5* (128), 105592–105599.
- (58) Wei, Q.; Mukaida, M.; Naitoh, Y.; Ishida, T. Morphological change and mobility enhancement in PEDOT: PSS by adding cosolvents. *Advanced materials* **2013**, *25* (20), 2831–2836.
- (59) Romele, P.; Gkoupidenis, P.; Koutsouras, D. A.; Lieberth, K.; Kovacs-Vajna, Z. M.; Blom, P. W. M.; Torricelli, F. Multiscale real time and high sensitivity ion detection with complementary organic electrochemical transistors amplifier. *Nat. Commun.* **2020**, *11* (1), 3743.
- (60) Sun, H.; Vagin, M.; Wang, S.; Crispin, X.; Forchheimer, R.; Berggren, M.; Fabiano, S. Complementary logic circuits based on high-performance n-type organic electrochemical transistors. *Adv. Mater.* **2018**, *30* (9), 1704916.
- (61) Yang, C.-Y.; Tu, D.; Ruoko, T.-P.; Gerasimov, J. Y.; Wu, H.-Y.; Harikesh, P. C.; Massetti, M.; Stoeckel, M.-A.; Kroon, R.; Muller, C.; Berggren, M.; Fabiano, S. Low-Power/High-Gain Flexible Com-

mentary Circuits Based on Printed Organic Electrochemical Transistors. *Advanced Electronic Materials* **2022**, *8* (3), 2100907.

(62) Romele, P.; Ghittorelli, M.; Kovacs-Vajna, Z. M.; Torricelli, F. Ion buffering and interface charge enable high performance electronics with organic electrochemical transistors. *Nat. Commun.* **2019**, *10* (1), 3044.

(63) Sun, H.; Vagin, M.; Wang, S.; Crispin, X.; Forchheimer, R.; Berggren, M.; Fabiano, S. Complementary Logic Circuits Based on High-Performance n-Type Organic Electrochemical Transistors. *Adv. Mater.* **2018**, *30* (9), 1704916.

(64) Rashid, R. B.; Du, W.; Griggs, S.; Maria, I. P.; McCulloch, I.; Rivnay, J. Ambipolar inverters based on cofacial vertical organic electrochemical transistor pairs for biosignal amplification. *Science Adv.* **2021**, *7* (37), eabh1055.

(65) Arnold, F. E.; Van Deusen, R. Preparation and properties of high molecular weight, soluble oxobenz [de] imidazobenzimidazoisquinoline ladder polymer. *Macromolecules* **1969**, *2* (5), 497–502.

(66) Wu, J.; Rui, X.; Wang, C.; Pei, W. B.; Lau, R.; Yan, Q.; Zhang, Q. Nanostructured conjugated ladder polymers for stable and fast lithium storage anodes with high-capacity. *Adv. Energy Mater.* **2015**, *5* (9), 1402189.

Recommended by ACS

Tuning Threshold Voltage of Electrolyte-Gated Transistors by Binary Ion Doping

Kyung Gook Cho, Keun Hyung Lee, *et al.*

OCTOBER 27, 2022
ACS APPLIED MATERIALS & INTERFACES

READ 

Low-Voltage Organic Transistors with Carrier Mobilities over $10 \text{ cm}^2 \text{V}^{-2} \text{s}^{-1}$ Using Six-Branched Organic Azide

Myeongjae Lee, BongSoo Kim, *et al.*

NOVEMBER 17, 2022
CHEMISTRY OF MATERIALS

READ 

Photogated Synaptic Transistors Based on the Heterostructure of 4H-SiC and Organic Semiconductors for Neuromorphic Ultraviolet Vision

Xiao Liu, Deren Yang, *et al.*

JANUARY 10, 2023
ACS APPLIED ELECTRONIC MATERIALS

READ 

Dynamic Model of the Short-Term Synaptic Behaviors of PEDOT-based Organic Electrochemical Transistors with Modified Shockley Equations

Haonian Shu, Xiaoxue Wang, *et al.*

APRIL 19, 2022
ACS OMEGA

READ 

Get More Suggestions >